https://doi.org/10.5194/egusphere-2024-2520
Preprint. Discussion started: 4 November 2024

SISSOMA (v1): modelling marine aggregate dynamics from production to export

Andre William Visser[1], Anton Vergod Almgren[1], and Athanasios Kandylas[1]

[1]VKR Centre for Ocean Life, National Institute of Aquatic Resources, Technical University of Denmark, Kongens Lyngby, Denmark

Correspondence: Andre William Visser (awv@aqua.dtu.dk)

Abstract. A mechanistic approach linking the population dynamics of plankton communities to the export of detrital material to the oceans interior, remains a largely unresolved component of global bio-geochemical models. We propose that the self-similarity of aggregation provides a tractable modelling framework for simulating the dynamics and sinking speed of natural marine particle aggregates. It provides a means to track both size and excess density of aggregates as they are formed and transformed by aggregation, degradation and fragmentation processes. A self-similarity parameter a in the range 1.8 to 2.1 is well supported by direct observations drawn from an extensive database of aggregate size and sinking speed. We provide a simple model, SISSOMA, that uses a 2 dimensional state-space representation of aggregate dynamics for which we conduct sensitivity analyses for the self-similarity parameter, stickiness, turbulent dissipation rate and the production rate of primary particles. The model provides size and density resolved estimates of the export flux of detrital material generated by a diverse community of primary producers. While open to improvement in several aspects, the model compares well with observations of aggregate size spectra covering the global ocean.

1 Introduction

The rain of particulate organic matter (POM) sinking from the surface to the ocean's interior constitutes a major pathway in global biogeochemical cycling (Volk and Hoffert, 1985; Buesseler et al., 2007). Together with active transport by vertically migrating organisms, it contributes to the ∼10 PgC/year export flux (∼ 20% of total marine primary production) that feeds the world's mesopelagic and benthic ecosystems and drives the biological carbon pump (Ducklow et al., 2001; Mouw et al., 2016). Yet, despite its central role and the fact that relevant physical theories have existed for more than 100 years (Stokes, 1851; Smoluchowski, 1918), a mechanistic description of POM sinking rates remains elusive leaving biogeochemical models largely at the mercy of empirically derived formulations that are not best suited for predictions under expected global change.

In part this is due to the tendency of model descriptions to focus on size as the preeminent variable controlling POM flux. After all, Stokes' law and its derivatives predict a strong size dependence on sinking speed (Clift et al., 1978; White, 1991),

https://doi.org/10.5194/egusphere-2024-2520
Preprint. Discussion started: 4 November 2024

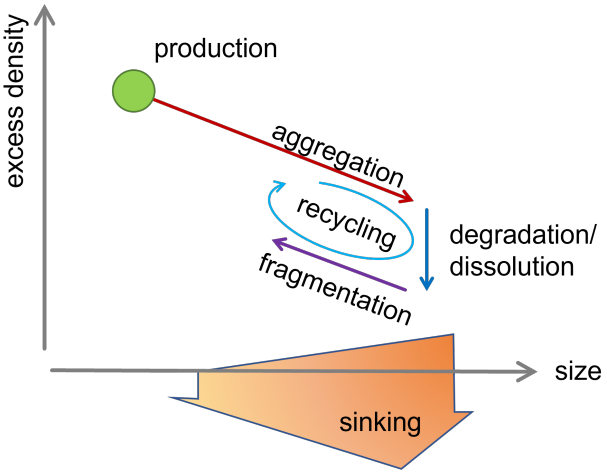

Figure 1. Aggregate dynamics depicted in 2 dimensional state space. Primary particles are produce in a specific size and density range. Aggregation, dissolution/degradation and fragmentation serve to redistribute aggregate mass within this phase-space. The distribution of aggregates eventually reaches steady state when the rate of supply is balanced by the sinking losses and losses due to dissolution/degradation.

and coagulation theory provides a theoretical framework for how aggregates grow in size (Burd and Jackson, 2009; Jackson and Burd, 2015). Further, with the advent of laser optics, aggregate size spectra are now routinely measured in the field. It is often commented however, that size is a poor predictor of sinking speed; aggregates of any size from microns to centimeters seemingly sink at any speeds from practically zero to several 1000s of meters per day (Iversen and Lampitt, 2020), prompting an abandonment of mechanistic approaches (Laurenceau-Cornec et al., 2020) in favour of more empirically derived formulations (Cael et al., 2021). In these considerations, the other key variable determining sinking speed, namely the excess density of aggregates is often sidelined. It is well understood for instance that ballasting (e.g. biogenic minerals, aolean dust (Iversen and Ploug, 2010; Iversen and Robert, 2015; Van der Jagt et al., 2018)) or buoyant material (transparent exopolymers TEP (Azetsu-Scott and Passow, 2004)) can radically change sinking speeds. Further porosity, a dynamic property of the aggregation process exerts a strong control on excess density (Laurenceau-Cornec et al., 2020; Jackson and Burd, 1998). While these processes are qualitatively well understood, only few modelling frameworks seek to systematically include aggregate excess density as a state variable (Jackson and Burd, 1998; Jokulsdottir and Archer, 2016). Within this context, there are 3 major controls on aggregate excess density; the inherent density of the primary particles from which the aggregates are formed, the aggregation process which traps increasing volumes of interstitial water thereby systematically reducing excess density, and dissolution and degradation processes that solubilize solid material from the aggregate matrix.

Here we propose a 2 dimensional state-space representation of a marine aggregate community (Fig. 1) where the dynamics are driven by three transformative processes; aggregation producing larger less dense aggregates, degradation/dissolution which reduces the solid mass (and hence excess density), and fragmentation. At a system level (e.g. the surface mixed layer), the model links the production of primary particles (e.g. dead and dying organisms, fecal pellets, aeolian dust etc.) to losses

https://doi.org/10.5194/egusphere-2024-2520
Preprint. Discussion started: 4 November 2024

through sinking, dissolution and degradation. While still relatively complex, each of the sub-processes can in principle be constrained from observations, parameterized and mechanistically formulated. What makes this framework particularly attractive is the development of size-based and trait-based models of plankton communities (Banas, 2011; Serra-Pompei et al., 2020; Serra-Pompei et al., 2022) which provide precisely the type of information (size and trait resolved primary productivity and zooplankton grazers) that can serve as input. Indeed a resolved particle aggregation model can provide a mechanistic link between emerging plankton community structure and export flux; one of the key unresolved issues of the biological carbon pump (Boyd and Newton, 1995; Bach et al., 2019).

The key concept we explore here is that aggregation is a geometrically self-similar process, such that the linear dimension r_{ioj} of an aggregate formed by the combination of two parent aggregates of linear dimension r_i and r_j respectively is given by:

$$r_{i\circ j} = (r_i^a + r_j^a)^{(1/a)} \tag{1}$$

That is, for the binary process of aggregation, r^a is an additive conservative property. This is not a new idea (Jackson, 1998; Wiesner, 1992) and arises from the general observation that aggregates display fractal characteristics (Alldredge and Gotschalk, 1988; Meakin, 1987; Logan and Wilkinson, 1990). We term a the self-similarity parameter, and note $a < 3$ in compliance with the observed increase in porosity under aggregation. We stress that a is not the fractal dimension of the aggregate. Neither is it an inherent property of aggregates and we will not attempt to use a to produce scaling laws as is usual in these considerations. e.g. (DeVries et al., 2014; Kriest and Evans, 1999; Cael et al., 2021). At this point we simply want to treat a as a parameter governing the binary process of aggregation.

Under geometric self-similarity, the mass of an aggregate produced by the combination of 2 aggregates of mass m_i and m_j can be deduced to be the sum of these two masses, plus a bit extra due to the inclusion of some fluid (density ρ_w) that occupies the expanded aggregate volume (increased porosity). Specifically,

$$m_{ioj} = m_i + m_j + \frac{4}{3}\pi(r_{ioj}^3 - r_i^3 - r_j^3)\rho_w \tag{2}$$

Here m is the total mass, not just the dry mass of the aggregate. It is convenient to recast this in terms of density of the aggregates, ρ_i, ρ_j, ρ_{ioj}, and their respective volumes, v_i, v_j and v_{ioj}. It follows that excess density

$$\rho_{ioj} - \rho_w = \frac{v_i}{v_{ioj}}(\rho_i - \rho_w) + \frac{v_j}{v_{ioj}}(\rho_j - \rho_w) \tag{3}$$

That is, aggregation produces a daughter particle whose excess density is the volume weighted mean of the excess density of the two parent particles. Eqs. (1) and (3) provide an iterative computational framework that can follow the size and excess density and hence sinking speed, of aggregates as they are formed and transformed from primary particles.

2 Observed state-space distributions.

The physics of sinking particulate matter is well understood in terms of a balance between buoyancy B and drag D forces (Clift et al., 1978), where the precise form of the balance depends strongly on Reynolds number R (White, 1991; Loth, 2008).

https://doi.org/10.5194/egusphere-2024-2520
Preprint. Discussion started: 4 November 2024

Specifically, the drag on an aggregate sinking at speed w transitions from a linear ($D \propto w$) to a quadratic ($D \propto w^2$) as R transitions from $R \ll 1$ (viscous regime) to $R \gg 1$ (inertial regime). Here Reynolds number is given by $R = 2rw/\eta$, with η being the kinematic viscosity of seawater. For a smooth, spherical, non-permeable particle of radius r, sinking speed is given by

$$w^2 = \frac{8}{3}\frac{\rho - \rho_w}{\rho_w}\frac{g\,r}{C} \tag{4}$$

where w is sinking speed, r the estimated spherical radius, g the gravitational acceleration, and C is an empirically derived drag coefficient. While there are several formulations, generally expressed as a function of Reynolds number, the most commonly used is

$$C = \frac{24}{R} + \frac{6}{1+\sqrt{R}} + 0.4 \tag{5}$$

White (1991). This, and similar formulas are robust for R up to about 10^5. As $R \to 0$, Eq. (4) returns the Stokes' law. We note that while there are additional physical factors effecting the drag coefficient, notably aggregate shape, surface roughness and permeability, these manifest as relatively small corrections, particularly for Reynolds numbers relevant for marine aggregates (Logan and Hunt, 1987; Dietrich, 1982; Laurenceau-Cornec et al., 2015).

Our approach is informed by the distribution of natural marine aggregates in size-density space. Excess density itself is not easily measured, but can be back-calculated (Engel et al., 2009; Iversen and Ploug, 2010) from sinking speed and size observations. Indeed, from Eq. (4) it follows

$$\rho - \rho_w = \rho_w \frac{3}{8}\frac{Cw^2}{gr} \tag{6}$$

We estimate excess density (Fig. 2) from existing databases (Laurenceau-Cornec et al., 2015; Cael et al., 2021) together with additional observations (Gärdes et al., 2011; Bach et al., 2019; Iversen and Lampitt, 2020). The preponderance of observations correspond to $R < 100$ and thus lie well within the range where Eq. (5) is valid.

In general, sinking speeds tend to increase with particle size albeit with a high degree of variance (Fig. 2.a). Indeed there is no real statistically significant relationship between w and r overall, nor within observational sub-sets (Laurenceau-Cornec et al., 2015). Estimated excess density for these observations (Fig. 2.b) in contrast, shows a marked decrease with aggregate size, consistent with a commensurate increase in porosity, a signature of the self-similarity of aggregation processes. Even so, estimated excess densities vary considerably within size classes; over 3 orders of magnitude for all observations and about 1 order of magnitude for individual observational studies.

Under special conditions, self-similarity makes quite strong predictions on how aggregate properties (e.g. mass, density, porosity) scale with size. Specifically, for a monoculture of primary particles of size r_0 and density ρ_0, and in the absence of degradation, dissolution, or fragmentation, then aggregates' excess density follows a power law:

$$\rho(r) - \rho_w = (\rho_o - \rho_w)\left(\frac{r}{r_0}\right)^{a-3} \tag{7}$$

Under these conditions, the aggregation vector in the Fig. 1, would have an expected slope $a - 3$.

https://doi.org/10.5194/egusphere-2024-2520
Preprint. Discussion started: 4 November 2024

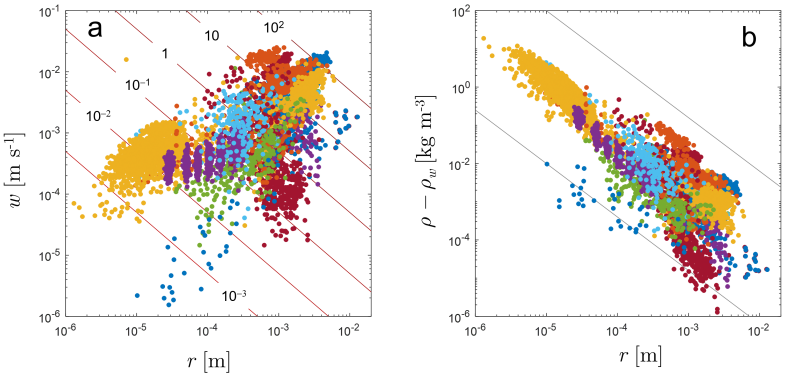

Figure 2. (a) Aggregate sinking speed (w) observed in a large number of studies (cf. Table 1) as a function of estimated spherical radius (r) and (b) the excess density ($\rho - \rho_w$) calculated from observed sinking speeds using a modified Stokes law. Colors represent different studies. The lines in panel (a) are contours of Reynolds number ranging from 100 to 0.001. The grey lines in panel (b) indicate a log-log slope of -1.4.

Within the set of field and laboratory observations reported in Table 1, a subset meet suitable criteria that can reveal such a relationship. For instance, Iversen and Ploug (2010) conducted laboratory studies of aggregates from relatively fresh monocultures of the chain forming diatom *Skeletonema costatum* and the coccolithophore *Emiliania huxleyi*, and mixtures of the two. Log-log regressions on these indicate b in the range -1.2 to -1.0 i.e. a in the range 1.8 to 2.0. Other laboratory observations that have avoided degradation and extraneous manipulations with TEP and dust indicate similar relationships with b in the range $[-1.2, -0.9]$ (Engel and Schartau, 1999; Engel et al., 2009; Laurenceau-Cornec et al., 2015).

These values are consistent with laboratory experiments for non-biological particle aggregation Lin et al. (1989) for which a ranges between 1.8 and 2.1. The lower value corresponds to a relatively porous structure that arises when aggregates are built-up of very sticky, similarly sized particles that combine immediately on contact. The value $a = 2$ corresponds to a random walk arrangement in 3 dimensions, and has been used in previous model settings (Jackson and Burd, 1998; Jokulsdottir and Archer, 2016). From these considerations, it appears that a in the ranges 1.8 to 2.1 is a reasonable choice.

It is also clear that a large number, indeed the majority, of studies listed in Table 1, exhibit slopes b that are spread across a much broader range. These studies all follow quite different experimental (e.g. natural aggregates, lab cultures, manipulations with ballast material) and observational procedures (e.g. *in situ* cameras, roller tanks, vertical flow systems). In some instances it can be argued that the observation method is poorly designed to capture the characteristics of the full aggregate community. Roller tanks for instance preferentially generate large, fast-sinking aggregates (Jackson, 2015) producing particle size spectra that are not representative of natural aggregate communities. Perhaps more important is the heterogeneity of the primary particles. In some experimental setups, ballasting material of considerably different excess densities are present or introduced. Further, natural plankton communities are seldom mono-cultures, and are generally composed of unicellular organisms covering a range of sizes and densities; some with shells and spines, some vacuolated, some chain-forming. In any given size

https://doi.org/10.5194/egusphere-2024-2520
Preprint. Discussion started: 4 November 2024

range, the aggregate community will be an ad-mixture derived from different primary particles. Furthermore, as aggregates degrade and fragment, smaller, less dense aggregates come into the mix – grist to the mill – so that aggregate density, and hence sinking speed, will exhibit a relatively broad distribution at any given aggregate size. We must therefore conclude that while the majority of observations plotted in Fig. (2) are perfectly fine in relating the sinking speed to the size of an aggregate, methodological issues mean that they remain mute on any self-similarity in the underlying aggregation process. Seen in this light, it appears that the variance of excess density (Fig. 2.b) is composed of two elements; a general negative slope being due to increased aggregate porosity with size, and an inherent variability due to the excess density of primary aggregate material.

3 The SISSOMA Model

The physical setting we consider is a surface mixed layer of depth h where aggregates are produced from a range of primary particles, transformed and sink out according to the dynamics described in Fig. (1). We introduce the state variable $\mathsf{s} = (r, \rho - \rho_w)$ describing aggregate attributes, and note that all of the information required to estimate sinking speed is contained in s. We denote a binary combination of aggregates as $\mathsf{s}_{ioj} = c^\circ(s_i, s_j)$ and it is also convenient to introduce the function $c^\star$ such that $\mathsf{s}_i = c^\star(\mathsf{s}_{ioj}, \mathsf{s}_j)$ returns the state of a parent aggregate given the daughter and other parent. These functions follow directly from Eqs. (1) and (3).

The equation for aggregate dynamics can be written as:

$$
\begin{aligned}
\frac{\partial}{\partial t}\mathsf{N}(\mathsf{s},t) = \\
& q_{m:c}\mathsf{P}(\mathsf{s},t) \\
& + \frac{\alpha}{2}\int_{\mathsf{S}} \beta(\mathsf{s}', c^\star(\mathsf{s},\mathsf{s}'))\, \mathsf{N}(c^\star(\mathsf{s},\mathsf{s}'),t)\, \mathsf{N}(\mathsf{s}',t)\, d\mathsf{s}' \\
& - \alpha\, \mathsf{N}(\mathsf{s},t) \int_{\mathsf{S}} \beta(\mathsf{s},\mathsf{s}')\, \mathsf{N}(\mathsf{s}',t)\, d\mathsf{s}' \\
& - \mathsf{N}(\mathsf{s},t)\, \frac{w(\mathsf{s})}{h} \\
& - \psi(\mathsf{s})\, \mathsf{N}(\mathsf{s},t) + \int_{\mathsf{S}} \psi(\mathsf{s}')\, \mathsf{N}(s',t)\, \theta(s,s')\, ds' \\
& - \frac{\partial \mathsf{s}}{\partial t} \cdot \frac{\partial \mathsf{N}}{\partial \mathsf{s}}
\end{aligned}
\tag{8}
$$

where $\mathsf{N}(\mathsf{s})d\mathsf{s}$ is the number of aggregates in a small region of state space $[\mathsf{s}, \mathsf{s}+d\mathsf{s}]$. The first term ($q_{m:c}\mathsf{P}$) represents production rate of primary particles with different state space characteristics (cf Table 2 for a listing of variables and units). The following two terms are classic coagulation theory (Smoluchowski, 1918) rewritten for multidimensional state space (denoted S), where $\beta(\mathsf{s},\mathsf{s}')$ is the encounter kernel for two aggregates in state s and s' respectively and α is the stickiness (i.e. the probability that on contact, aggregation occurs). The fourth term is a simplified sinking loss term, where $w(\mathsf{s})$ is the sinking speed (Eq. 4), and h is the thickness of the surface layer. The fifth and sixth terms represent fragmentation where $\psi(\mathsf{s})$ is a state specific

https://doi.org/10.5194/egusphere-2024-2520
Preprint. Discussion started: 4 November 2024

fragmentation rate and $\theta(\mathsf{s},\mathsf{s}')$ is a partitioning function. This general form can accommodate both physical fragmentation or partial consumption by zooplankton. The final term represents processes that affect internal changes in aggregate state such as degradation, dissolution and compaction. Note that since s is a multi-dimensional variable, the last term is actually a vector product. Similar expressions have been introduced previously (Burd and Jackson, 2009; Jackson and Burd, 2015) albeit for a single state parameter (usually aggregate mass) and without explicit representations of fragmentation or degradation.

Our model SISSOMA is essentially a numerical implementation of Eq.(8) in discetized state space. Its name derives from the Greek word "$\sigma\acute{\upsilon}\sigma\sigma\omega\mu\alpha$" which literally means "aggregation" ($\sigma\upsilon\nu$ - "addition" + $\sigma\acute{\omega}\mu\alpha$ - "body"). In a more liberal interpretation of this word, SISSOMA encompasses the values of unity, collaboration and support between people working towards a common goal.

It is convenient to introduce two transformed variable (x,z) that map to $(r,\rho-\rho_w)$ as:

$$r = r_o\delta^x, \quad \rho-\rho_w = \rho_o\lambda^z\delta^{(a-3)x} \tag{9}$$

Here x is a logarithmic scaling of aggregate size, and z a stretched logarithmic scaling of excess density. The factor $\delta^{(a-3)x}$ takes advantage of the reduction of density by aggregation and expands the density resolution for large aggregates. Fig (3) presents the excess density and sinking speed for a given (x,y) state space. The mapping in Eq. (9) essentially seeks to efficiently cover the range of observations populating Fig (2b).

Key variables in the model are the matrices N and M representing the number of aggregates and their total dry mass respectively within bins in discretized (x,z) state space. Suitable range choices for $x\in[0,X]$ and $z\in[0,Z]$, scaling factors r_o [µm] and ρ_o [kg m^{-1}], and logarithmic intervals δ and λ allow for a relatively complete representation of the aggregate community within computationally convenient dimensions of N and M. Total aggregate dry mass M and number density N are related by $\mathsf{M}=\mathsf{m}'\circ\mathsf{N}$ where $\circ$ represents piece-wise matrix product and m' is the mean dry mass of an aggregate within each bin.

Aggregation is computationally the most complex aspect of the model as it involves an off-set binary convolution of N in state space. Performing binary convolution calculations is greatly facilitated by self-similarity. Specifically, the ordinates of an aggregate produced from the combination of (x_i,z_i) and (x_j,z_j) is given by:

$$\begin{aligned} x_{i\circ j} &= \frac{1}{a\ln\delta}\ln\left(\delta^{ax_i}+\delta^{ax_j}\right) \\ z_{i\circ j} &= \frac{1}{\ln\lambda}\ln\left(\lambda^{z_i}\delta^{a(x_i-x_{i\circ j})}+\lambda^{z_j}\delta^{a(x_j-x_{i\circ j})}\right) \end{aligned} \tag{10}$$

It follows that the combination of aggregates from any two domains of identical shape in (x,z) state space will be confined to a third identically shaped domain. The model utilizes this feature on a regular (x,z) grid in optimizing the algorithm architecture (Appendix A).

Aggregation is governed by encounter kernels β and stickiness α and follows standard formulations (Burd and Jackson, 2009; Jokulsdottir and Archer, 2016) with three specific processes (Brownian motion, differential settling and turbulent shear) contributing to the encounters. We use the rectilinear formulations (Burd and Jackson, 2009) which are mainly functions of particle size and sinking speed. The most important environmental variable is turbulent dissipation rate (denoted ε, units m^{3}s^{-2}) which can vary over several orders of magnitude for natural marine systems (Visser et al., 2001).

https://doi.org/10.5194/egusphere-2024-2520
Preprint. Discussion started: 4 November 2024

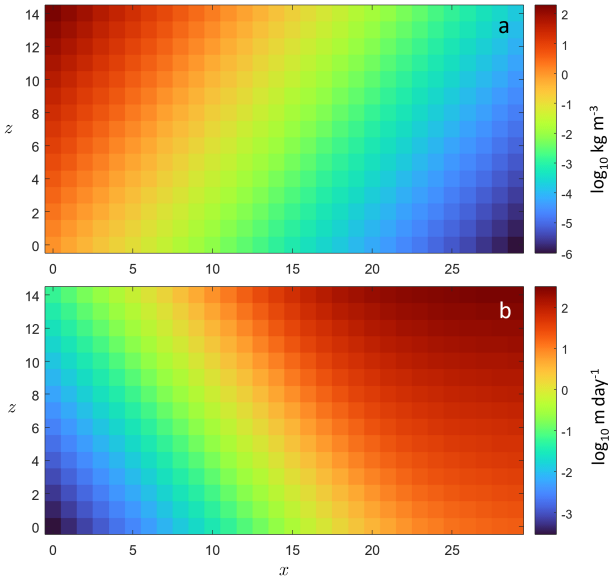

Figure 3. (a) Aggregate excess density $\rho - \rho_w$ [kg m^{-3}] and sinking speed w [m day$^-$1] for a $(X, Z) = (30, 15)$ aggregate state-space. Ordinate convention: the full range of x spans the interval $[0, X]$ in $X - 1$ bins, and similar for z. The ordinate convention we choose here is that the ordinates (x, z) implies the bin spanning $([x, x + 1], [z, z + 1])$. Actual scale r_0, δ so that $r \in [10^{-6}, 1]$ m and ρ

We assign the productivity P of primary particles to be consistent with a typical plankton community. The total productivity of primary particles in terms of carbon is $\overline{\mathsf{P}} = \int_{\mathsf{S}} \mathsf{P} d\mathsf{s}$. We relate this to the rate at which dry mass is being produced through the parameter $q_{m:c}$, dry mass to carbon mass ratio. For this work we use $q_{m:c} = 2.5$ (Parsons et al., 1961) although it can be as high as 8 for diatom cells (Sicko-Goad et al., 1984) and likely higher still for copepod fecal pellets.

We simulate degradation as a drift of particle numbers to lower density bins, implemented as:

$$\left.\frac{\partial \mathsf{N}}{\partial t}\right|_{\text{deg}} = \frac{\partial \rho'}{\partial t}\frac{\partial \mathsf{N}}{\partial \rho'} = -\frac{\gamma}{\ln \lambda}\frac{\partial \mathsf{N}}{\partial z} \tag{11}$$

Here, γ is the degradation rate, and it can be shown (Appendix B) that the z ordinate of an aggregate follows $dz/dt = -\gamma/\ln\lambda$. In this, degradation acts only on excess density. We set $\gamma = 0.1$ day^{-1} consistent with a range of studies (Kiørboe, 2001; Cavan and Boyd, 2018; Bach et al., 2019) although more recent direct observations suggest a lower value ($\gamma < 0.03$) (Belcher et al., 2016). It should also be noted that there is considerable variation due to for instance, temperature effects, lability of organic material and/or dissolution of mineral ballast. This formulation conserves total aggregate number $\overline{\mathsf{N}} = \int_{\mathsf{S}} \mathsf{N} d\mathsf{s}$, but not total mass $\overline{\mathsf{M}} = \int_{\mathsf{S}} \mathsf{M} d\mathsf{s}$. Indeed,

$$\left.\frac{\partial \overline{\mathsf{M}}}{\partial t}\right|_{\text{deg}} = -\gamma \overline{\mathsf{M}} \tag{12}$$

Finally fragmentation is simulated simply as a rate at which aggregate mass is transported to smaller sizes classes. We implement this as an increasing function of aggregate size. Further, it is intuitively understood that fragmentation increases as

https://doi.org/10.5194/egusphere-2024-2520
Preprint. Discussion started: 4 November 2024

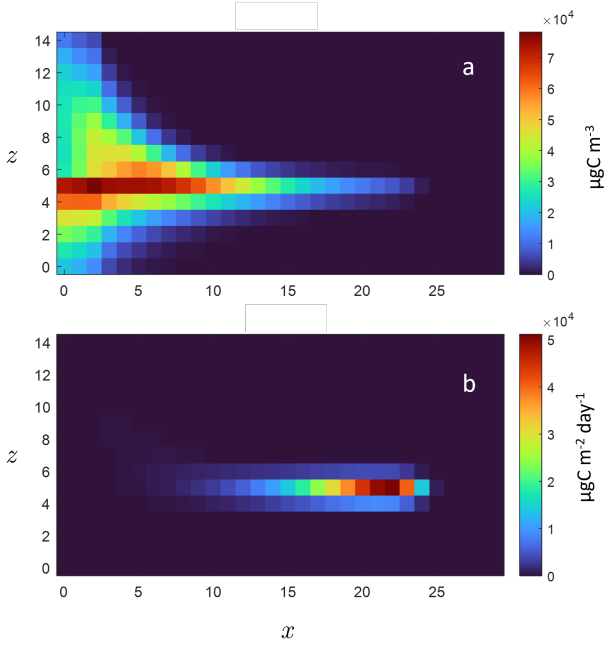

Figure 4. Distribution of (a) total dry mass $\mathsf{M}(x,z)$ [μg m^{-3}] and (b) flux $\mathsf{F}(x,z)$ [μg C m^{-2} day^{-1}] over aggregate state-space. Steady state solution for self similarity a = 2, stickiness α = 0.1, turbulent dissipation rate ε = 10^{-6} [m^{-2} s^{-3}] and total productivity $\overline{\mathsf{P}} = 2 \times 10^6$ [μg C m^{-2} day^{-1}]. The total productivity is spread evenly over all densities in the three smallest size classes. That is $\mathsf{P}(0,z)$ =$\overline{\mathsf{P}}/(3Z)$ for all z, and 0 otherwise.

turbulent stresses increase. Of the processes considered, fragmentation remains the least well constrained; aggregates appear resistant to mechanical shear (Alldredge et al., 1990), and fragmentation appears to be chiefly mediated by metazooans through handling and feeding appears to be important (Dilling and Alldredge, 2000) and by microbial "mining" and dissolution of adhesive material. We set the fragmentation rate at $\psi_0 = 0.5$ day^{-1} for large porous aggregates, a value consistent with observations (Briggs et al., 2020). Specifically, we set

$$\psi(\mathsf{s}) = \psi_0 \frac{\varepsilon}{\varepsilon_c} \left(\frac{r}{r_c} \right)^3 \frac{1-\phi}{1-\phi_c} \tag{13}$$

where $(\varepsilon_c, r_c, \phi_c)$ are reference turbulence, size and porosity respectively where fragmentation rate is ψ_0. Given the uncertainty in fragmentation processes, we choose a simple redistribution rule where the mass from fragmented aggregates is simply distributed evenly across all smaller size classes. Specifically, the mass of fragments $d\mathsf{M}(x,z) = \psi(x)\mathsf{M}(x,z)$ from $\mathsf{s} = (x,z)$ is distributed evenly across all bins $\mathsf{s} = (x',z)$ for $0 > x' > x$.

https://doi.org/10.5194/egusphere-2024-2520
Preprint. Discussion started: 4 November 2024

4 Results and sensitivity

We present a series of simulations for a fixed rate of primary particle production (size range 1 to 30 μm in radius, excess density range 1 to 200 kg m^{-3}) that corresponds to a mixed community of unicellular auto- and heterotrophic plankton ranging from cyanobacteria to diatoms. Table 2 contains relevant nomenclature, parameter settings and ranges. Simulations were run to quasi-steady state (i.e. relative differences between successive daily estimates (normalized root-mean-square deviation) were $< 10^{-6}$) using a MATLAB ode solver. Four sets of parameters (self-similarity, stickiness, turbulent dissipation rate, and total production rate) were varied between runs and the emerging aggregate community was characterized by its size spectrum and size resolved export flux. All simulations assumed a mixed layer depth of $h = 50$ m. The results of one such run is presented in Fig (4) for the same state space as shown in Fig. (3). The steady-state dry mass distribution (Fig 4a) is dominated by aggregates in the ~ 10 μm size range and and excess density of ~ 100 g m^{-3} (Fig. 3). These aggregates have slow sinking speeds of about ~ 1 cm day^{-1}. The export flux in contrast is dominated by cm scale aggregates (Fig. 4.b). While these aggregates have much lower excess density ~ 1 g m^{-3} because of their increased porosity, they still have sinking speeds of the order ~ 10 m day^{-1} (Fig. 3).

Results for the sensitivity analysis are presented in Fig (5), and the numerical code that produced it can be found in the supplementary material. Particle size spectra

$$n(r) = \frac{1}{dr(x)} \sum_z \mathsf{N}(x,z) \tag{14}$$

were estimated in the normal manner (Burd and Jackson, 2009) as per size bin width $dr(x)$ and provide a macroscopic measure of the underlying dynamics of production, transformation and sinking. Measurements of such spectra are routinely made and often conform to a power law of the form $n(r) \sim r^p$. Observations (Stemmann et al., 2008; Guidi et al., 2009; Reynolds and Stramski, 2021) from different oceanic regions and spanning aggregate sizes from microns to centimeters, show that p ranges from -2 to -6 and cluster around -3 to -4 in the surface ocean. For our model simulations (Fig. 5:b,d,f), all runs exhibited particle size spectra slopes of about -4 for aggregates from 1 to several 100s of μm in size.

The flux distributions

$$f(r) = \frac{1}{h\overline{\mathsf{P}}} \sum_z \mathsf{M}(x,z) \circ \mathsf{w}(x,z) \tag{15}$$

are the flux contributions summed over different excess density bins, reported within aggregate size bins and normalized with regards total primary particle production $\overline{\mathsf{P}}$. The shape of $f(r)$ is universally dome-shaped with very little flux at either small (low sinking speed) or large (low total mass) aggregate sizes. The peak of the flux distribution, and to some extent its width, varies with self-similarity, stickiness and turbulent dissipation rate. Low self-similarity indices for instance, push the flux distribution towards larger aggregate sizes, as do high turbulent dissipation rates. Stickiness by contrast has a relatively minor influence on the flux distribution. Maximum flux appears to be associated with a steepening of the particle size spectrum $n(r)$.

The total export flux, defined as

$$\mathsf{F} = \frac{1}{h\overline{\mathsf{P}}} \sum_{x,z} \mathsf{M}(x,z) \circ \mathsf{w}(x,z) \tag{16}$$

https://doi.org/10.5194/egusphere-2024-2520
Preprint. Discussion started: 4 November 2024

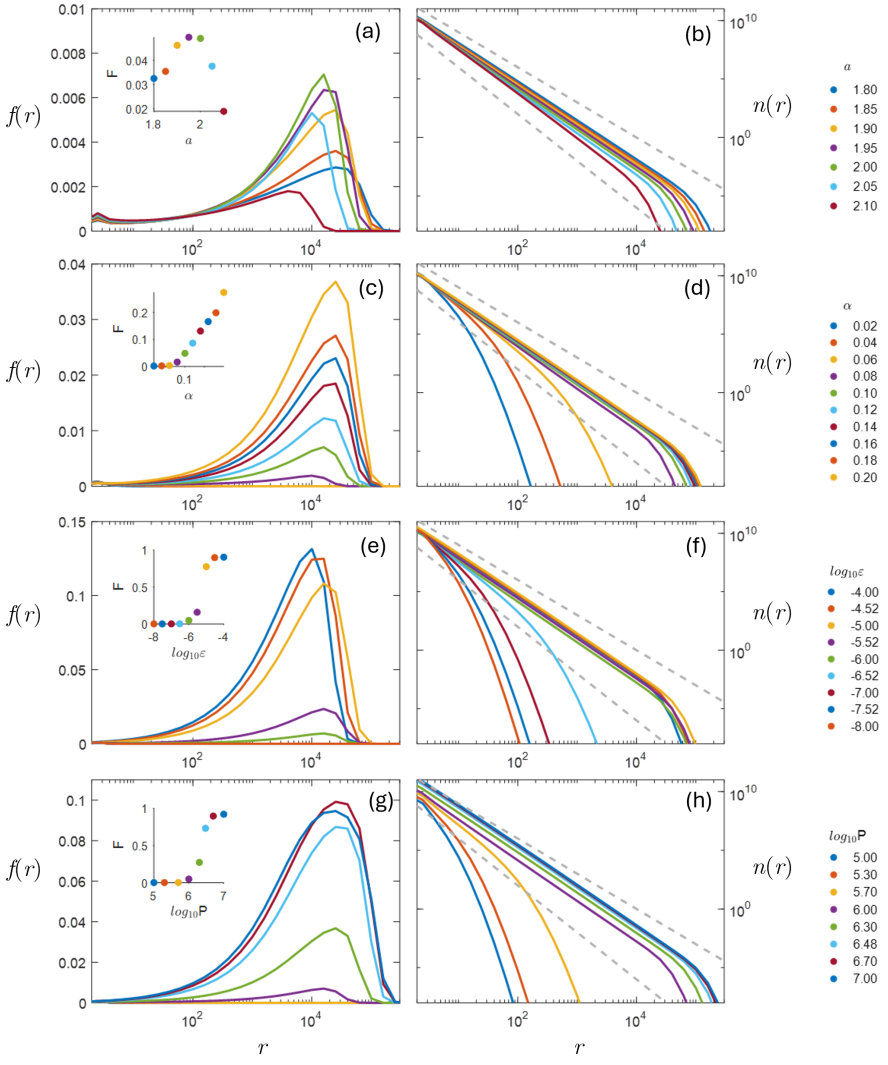

Figure 5. Aggregate community structure at steady state; $f(r)$ size resolved normalized export flux (a,c,e,g) and $n(r)$ particle size spectra (b,d,f,h) for a range of different a self-similarity parameters (a,b), α stickiness coefficients (c,d), ε turbulent dissipation rates [m^2 s^{-3}] (e,f), and P total productivity [μgC m^{-2} day^{-1}]. The insets in (a,c,e,g) show the total flux F [μgC m^{-2} day^{-1}] with respect to the various parameter settings. Dissipation rates are related to encounter rate β as given in Burd and Jackson (2009). Dashed lines in (b,d,f,h) indicate log-log slopes of -3 and -4.

is shown in the inset on the size-flux plots as a function of the sensitivity parameters (Fig. 3.a,c,e,g). Total export exhibits a strong nonlinear dependence on total productivity, dissipation rate, and to a slightly lesser degree on stickiness. This type of a nonlinear relationship is consistent with the idea of "critical cell concentration" (Jackson, 1990), with the rate of aggregation being roughly proportional to the square of the cell concentration. That is, for low primary particle concentration, the rate of

https://doi.org/10.5194/egusphere-2024-2520
Preprint. Discussion started: 4 November 2024

aggregate formation is slow, so most POC mass sinks slowly with a high degree of remineralization before it is exported. As concentration increases, more mass is shunted to larger fast sinking particles with a smaller faction being remineralized in the surface ocean, resulting in a larger overall proportion of the production being exported. The same holds true for increasing turbulence and stickiness, both of which increase the rate of large, fast-sinking aggregate formation.

We have argued that a universal self-similarity index a, if it exists, is relatively well constrained within the range $[1.8, 2.1]$. While the form of the exported flux $f(r)$ varies significantly within this range (Fig. 3.a), the total flux appears is to be relatively insensitive (Fig. 3.a inset). With regards variation in the characteristics of the export flux, the peak of the flux distribution (Fig. 3.a) ranges over an order of magnitude in aggregate size, from 300 to 3000 μm. Further, the flux distribution range is much narrower for high self-similarity indices, a feature that is exacerbated given the logarithmic scaling of the size bins. In contrast, total flux F, remains virtually the same across all these self similarity values. Indeed, the self similarity parameter has counteracting effects on sinking speed in terms of aggregate size and excess density (large a produce small but low porous aggregates and vice versa). The sinking speeds for aggregates in the flux maxima (Fig. 3.a) vary only modestly, from 10 to 20 m day^{-1} across all values of the self-similarity parameter. It should be noted that the export flux distribution in terms of aggregate size, excess density and sinking speed sets many of the key characteristics of the subsequent flux attenuation curve within the mesopelagic (e.g. remineralization length scale Cavan et al. (2017) and subsequent sequestration time scales Boyd et al. (2019)). While we cannot at this time provide argumentation to further constrain of the self-similarity parameter, we have put in place a mechanistic model that can guide empirical studies to improve resolution.

5 Discussion

The modelling framework we propose is designed specifically to track both size and excess density throughout an emerging aggregate community. We purposefully present the model itself in its simplest form. In this we are mindful that overly complex models become increasingly inscrutable, and unattractive for integration into higher level computational products. There are, however, aspects that should be further explored. For instance, a more rigorous approach would include porosity as an independent state variable (i.e. moving to a 3 dimensional state space) for which combination rules similar to Eqs. (1) and (3) can be derived. This would allow a more robust implementation of degradation and fragmentation. Degradation for instance is characterized here as a single parameter controlling the dissolution of the both organic and mineral components of the aggregate. Clearly this simplification could be improved on but would require a distinction between organic and inorganic aggregate components (i.e. and extra dimension). The organic components itself is a mixture of compounds with variable lability. These characteristics of the aggregate could also be simulated, but with the cost of extra dimensions. Further we simulate a single surface layer, where we assume uniform dynamics throughout, an obvious simplification that could be improved on. Conceptually at least, it is relatively straightforward to provide depth resolution for different production and turbulence regimes by stacking layers with aggregate exchange being provided by vertical fluxes and mixing.

While still complex in many aspects, the model hints at certain features that could be leveraged to provide a simpler, more computationally attractive model descriptions. It is worth noting for instance, that both dry mass distribution and export flux

https://doi.org/10.5194/egusphere-2024-2520
Preprint. Discussion started: 4 November 2024

converge at large aggregate sizes (x ordinate) to a relatively uniform z value (Fig. 4). This is a feature that is repeated for most parameter settings. A constant $z \approx z_c$ indicates that particle dynamics are dominated by aggregation / fragmentation, and where excess density is primary controlled by increased porosity. The value of z_c appears to be set within a few logarithmic size increments of the primary particle production range, indicating a convergence of primary particles to a characteristic "proto" aggregate confined to a sub-range of size and excess density, after which aggregation serves primarily to grow aggregates until they sink out of the surface mixed layer. That is, between primary particle and proto-aggregate, dynamics are dominated by production, degradation and aggregation, while from proto-aggregate on it is primarily aggregation, fragmentation and export that drive the dynamics. Indeed, if a systematic relationship can be found between production, aggregation and degradation and the characteristic of the proto-aggregate, then much of the modelling effort can be reduced.

More than anything, the poor ability to estimate the sinking speed of marine aggregates stems from the high variability of their excess density. Other factors, like shape, surface roughness and the through flow of interstitial fluid have been suggested, but these contribute at most a factor of 2 to sinking speed corrections. This is negligible compared to the orders of magnitude variance (yet alone a potential change in sign) exhibited in the excess density. All manners of primary particles are introduced into the surface ocean by primary producers, sloppy feeding, fecal matter and aeolian dust deposits. Further, the constituent components of detritus vary significantly in excess density (relative to seawater, 1027 kg m^{-3}) ranging from positively buoyant e.g. TEP in the range -200 to -300 kg m^{-3} (Azetsu-Scott and Passow, 2004) and lipids around -100 kg m^{-3} (Visser and Jónasdóttir, 1999) to near neutrally buoyant e.g. cytoplasm 3 to 70 kg m^{-3} (Tappan and Loeblich Jr, 1973), to very much negatively buoyant, e.g. coccoliths 1700 to 1900 kg m^{-3} (Toktamış et al., 2016), diatom frustules 1600 kg m^{-3} (Miklasz and Denny, 2010) and atmospheric dust (quartz, feldspar, calcite) approximately 1700 kg m^{-3}. It is a unique feature of SISSOMA that in can incorporate primary particles of any density and track their influence on the emerging aggregate community.

Stickiness is also a parameter that shows large variability in primary material. In SISSOMA, we assign a constant stickiness value to all aggregates from production to export. However, it has been shown that stickiness depends on the source of the primary particles ranging from 0.07 for dust mineral particles to 0.19 for TEP particles (Maerz et al., 2020). Furthermore, (Kiorboe et al., 1990) studying the growth of three diatom species, showed that the stickiness of their cells fluctuates following different patterns which are related to the nutrient availability and hence their growth phase. Hence, tracking the stickiness of the primary material throughout the aggregation process could provide a more robust prediction of the size distribution of the flux.

Of the processes specifically modelled, that with the greatest degree of uncertainty is fragmentation. This relates not just to the conditions that bring about the break-up of aggregates, but also how mass is redistributed into smaller aggregates. While promising techniques (Song and Rau, 2022; Hayashi et al., 2023) and algorithms (Gremion et al., 2021; Zahnow et al., 2011) are being developed to resolve this issue, it is hoped that SISSOMA can prove a useful platform for development and implementation.

Further, temporal aspects such as annual cycles of productivity, turbulence and mixed layer depth are yet to be explored. The presented sensitivity analyses are based on a marine aggregate community at a steady state. However, marine ecosystems, especially in high latitudes, are characterized by strong seasonal cycles of not only net primary productivity but also turbu-

https://doi.org/10.5194/egusphere-2024-2520
Preprint. Discussion started: 4 November 2024

lence, plankton community structure (both primary producers and grazers), which individually and in concert,influence production of POM and its export to the ocean's interior. We are currently coupling SISSOMA with NUM (Nutrient-Unicellular-Multicellular), a global, trait-based model of plankton dynamics (Andersen and Visser, 2023), to provide better insight into the connection between the plankton community structure and the carbon export flux in time and space.

Much of the literature concerning the fractal dimensions of aggregates has been built on the restrictive assumptions of irreversibility and uniform primary particles (Meakin, 1987; Lin et al., 1989) which leads to the rather handy definition that the fractal dimension of aggregates a' can be found from their mass-size relationship $m \sim r^{a'}$ (Meakin, 1987; Burd and Jackson, 2009). At the same time, aggregates found in the marine environment have been deemed to be fractal objects in that they display fractal type properties (Alldredge and Gotschalk, 1989; Logan and Wilkinson, 1990); an increase in porosity and a decrease in excess density as a function of size for instance. There is, however, a disconnection between these two concepts, namely that aggregation in the marine environment is not irreversible; aggregates degrade and fragment, and they are not composed of identical primary particles, either in size or excess density. Confining the concept of self-similarity to the aggregation process, rather than as a property of the aggregates provides a platform where not only aggregation can be modelled, but also other important transformative processes including degradation and fragmentation.

Finally, our concept of self-similarity of aggregation, and a governing parameter constrained to the range 1.8 to 2.1 is certainly open to scrutiny, particularly given its impact on the emerging flux-size distribution. That there is some systematic control on aggregate size and density is evident in Fig. (2.b). How this is manifested in a particular setting is, however, highly variable. We argue that in part, this variability can be accounted for through the aggregation process for which we provide a mechanistic description. A large part of the variance remains, however, and reflects the vastly different excess densities of the primary material from which the aggregates derive. Failure to recognize the variability in the density of primary material and how this propagates through an aggregate community confounds efforts to estimate fluxes and attenuation length scales of particulate matter in the oceans.

6 Conclusions

Herein, we introduce a relatively simple algorithm, from which the evolving aggregate community can be modelled within a 2-dimensional state space, specifically the size, and excess density of aggregates. Most importantly, the algorithm depends only on a few fundamental parameters; the self-similarity parameter, stickiness, degradation and fragmentation rates. All other variables are fixed by the physical environment (e.g. turbulence, mixed-layer depth, viscosity, external ballasting material) and the plankton community (e.g cell size, density, production rate, grazers, TEP production) for which models of varying complexity exist. Given a production rate of primary particles, the algorithm yields estimates of the flux of POM aggregates from the surface ocean resolved in terms of size and density (and hence sinking speed). Conceptually, this provides a mechanistic link between models of marine ecosystem productivity and biogeochemical models of the world's oceans.

https://doi.org/10.5194/egusphere-2024-2520
Preprint. Discussion started: 4 November 2024

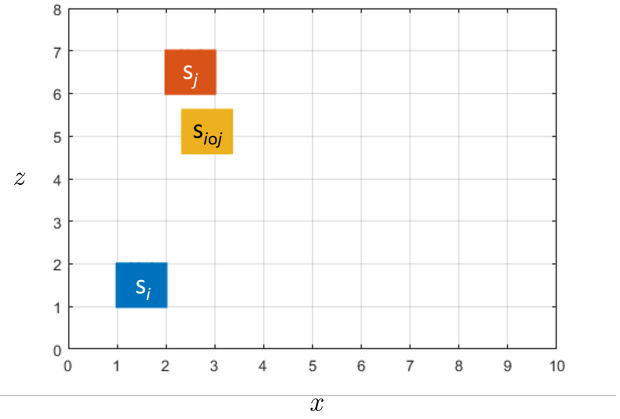

Figure A1. State-space aggregation. Aggregates formed by interactions between bins s_i and s_j will be found in the region s_{ioj} which will span, at most 4 bins in discretized state space.

Code and data availability. The model code and associated documentation for the simulations presented here is open source, and freely available on GitHub github.com/AndyWVisser/Aggregation and zenodo.org/records/12516012. All data used in estimating the excess density from size - sinking speed observations is vaialable at https://zenodo.org/records/6731389

Appendix A: Aggregation algorithm

Without loss of generality, aggregate state space can be defined in terms of transformed coordinates as

$$\mathsf{s} = \begin{bmatrix} x \\ z \end{bmatrix} \tag{A1}$$

from which it follows that the binary combination of aggregates can be written as

$$\mathsf{s}_{ioj} = c^\circ(\mathsf{s}_i, \mathsf{s}_j) = c^\circ\left(\begin{bmatrix} x_i \\ z_1 \end{bmatrix}, \begin{bmatrix} x_j \\ z_j \end{bmatrix}\right) = \begin{bmatrix} x_{ioj} \\ z_{ioj} \end{bmatrix} \tag{A2}$$

From Eq (10), it can be easily shown that

$$\mathsf{s'}_{ioj} = c^\circ(\mathsf{s}_i + \mathsf{s'}, \mathsf{s}_j + \mathsf{s'}) = \mathsf{s}_{ioj} + \mathsf{s'} \tag{A3}$$

where $\mathsf{s'}$ is an offset in state space. This means that any bounded region in state space convolved with another bounded region of the same shape will map to a third bounded region again of the same shape. Notably, within discretized state space, aggregation from two 1×1 bins maps to a third 1×1 bin (Fig A1). For the binary aggregation $\mathsf{s}_{ioj} \leftarrow c^\circ(\mathsf{s}_i, \mathsf{s}_j)$, the time rate of change of

https://doi.org/10.5194/egusphere-2024-2520
Preprint. Discussion started: 4 November 2024

particle numbers in appropriate state space bins are given by

$$
\begin{aligned}
d\mathsf{N}(\mathsf{s}_i) &= -\alpha\beta(\mathsf{s}_i,\mathsf{s}_j)\mathsf{N}(\mathsf{s}_i)\\
d\mathsf{N}(\mathsf{s}_j) &= -\alpha\beta(\mathsf{s}_i,\mathsf{s}_j)\mathsf{N}(\mathsf{s}_j)\\
d\mathsf{N}(\mathsf{s}^{00}_{ioj}) &= \alpha\beta(\mathsf{s}_i,\mathsf{s}_j)\mathsf{N}(\mathsf{s}_i)\mathsf{N}(\mathsf{s}_j)\xi^{00}\\
d\mathsf{N}(\mathsf{s}^{01}_{ioj}) &= \alpha\beta(\mathsf{s}_i,\mathsf{s}_j)\mathsf{N}(\mathsf{s}_i)\mathsf{N}(\mathsf{s}_j)\xi^{01}\\
d\mathsf{N}(\mathsf{s}^{10}_{ioj}) &= \alpha\beta(\mathsf{s}_i,\mathsf{s}_j)\mathsf{N}(\mathsf{s}_i)\mathsf{N}(\mathsf{s}_j)\xi^{10}\\
d\mathsf{N}(\mathsf{s}^{11}_{ioj}) &= \alpha\beta(\mathsf{s}_i,\mathsf{s}_j)\mathsf{N}(\mathsf{s}_i)\mathsf{N}(\mathsf{s}_j)\xi^{11}
\end{aligned}
\tag{A1}
$$

where

$$
\begin{aligned}
\mathsf{s}^{00}_{ioj} &= \begin{bmatrix} x^{00}_{ioj} \\ z^{00}_{ioj} \end{bmatrix} = \begin{bmatrix} \mathrm{floor}(x_{ioj}) \\ \mathrm{floor}(z_{ioj}) \end{bmatrix}\\
\mathsf{s}^{10}_{ioj} &= \mathsf{s}^{00}_{ioj} + \begin{bmatrix} 1 \\ 0 \end{bmatrix}\\
\mathsf{s}^{01}_{ioj} &= \mathsf{s}^{00}_{ioj} + \begin{bmatrix} 0 \\ 1 \end{bmatrix}\\
\mathsf{s}^{11}_{ioj} &= \mathsf{s}^{00}_{ioj} + \begin{bmatrix} 1 \\ 1 \end{bmatrix}
\end{aligned}
\tag{A2}
$$

and

$$
\begin{aligned}
\xi^{00} &= (x_{ioj} - x^{00}_{ioj})(z_{ioj} - z^{00}_{ioj})\\
\xi^{10} &= (1 - x_{ioj} + x^{00}_{ioj})(z_{ioj} - z^{00}_{ioj})\\
\xi^{01} &= (x_{ioj} - x^{00}_{ioj})(1 - z_{ioj} + z^{00}_{ioj})\\
\xi^{11} &= (1 - x_{ioj} + x^{00}_{ioj})(1 - z_{ioj} + z^{00}_{ioj})
\end{aligned}
\tag{A3}
$$

The total number of states s in discretized state space is $L = XZ$, from which it follows that the number of unique binary combinations is $K = (L+1)L/2$. For a moderate 10×8 state space resolution, $K = 3240$. Defining $k = 0, 1, 2, \ldots K-1$ as an ordinate counting combinations, $\ell = 0, 1, 2, \ldots L-1$ as an ordinate counting discrete states s, and

$$
\kappa(k) = \frac{1}{2}\left(2L + 1 - \sqrt{(2L+1)^2 - 8k}\right)
\tag{A4}
$$

it follows that

$$
\begin{aligned}
\ell_i &= \mathrm{floor}(\kappa(k))\\
\ell_j &= k - \ell_i L + \ell_i(\ell_i + 1)/2
\end{aligned}
\tag{A5}
$$

https://doi.org/10.5194/egusphere-2024-2520
Preprint. Discussion started: 4 November 2024

Further, each ℓ can be decomposed into x, z ordinates as:

$$x = \text{floor}(\ell/Z); \qquad z = \ell - xZ \tag{A6}$$

That is, each k is associated with a unique combination $(\ell_i, \ell_j) \leftrightarrow (x_i, z_i, x_j, z_j)$ from which the offset ordinates $(\ell^{00}_{ioj}, \ell^{01}_{ioj}, \ell^{10}_{ioj}, \ell^{11}_{ioj})$ for binary aggregation can be defined as in Eq. (A2). These provide a means of mapping indices for binary combinations, to state space and back. A consequence of the model architecture is that once a state space is defined, all coefficients determining the convolution process (encounter kernels β, offset indices $\ell^{00}_{ioj}, \ell^{01}_{ioj}, \ell^{10}_{ioj}, \ell^{11}_{ioj}$, and partitioning functions $\xi^{00}_{ioj}, \xi^{00}_{ioj}, \xi^{00}_{ioj}, \xi^{00}_{ioj}$) are fixed. That is, these need only be calculated once, stored in vectors of length K, and referenced via a lookup map.

Appendix B: Remineralization

For any aggregate we can express its density ρ as

$$\rho = \frac{m}{v} = \frac{m_d + m_w}{v} = (1-p)\rho_d + p\rho_w \tag{B1}$$

where p is the porosity, ρ_d is the density of the solid phase of the aggregate and ρ_w is the density of water. This leads to the expression for excess density ρ'

$$\rho' = \rho - \rho_w = \phi(\rho_d - \rho_w) \tag{B2}$$

where we have used $\phi = 1-p$. The simplifying assumption we make in this work is that within a short time step, reminealization removes dry mass from the aggregate, while the overall volume of the aggregate remains invariant. The volume of dry mass that is lost, is replaced by water thus increasing aggregate porosity p. The fundamental degradation process can be written as

$$\frac{dm_d}{dt} = -\gamma m_d \tag{B3}$$

Writing $m_d = v\phi\rho_d$ and assuming that the density of the dry mass phase remains invariant it follows that

$$\frac{d\phi}{dt} v\rho_d = -\gamma\phi v\rho_d \tag{B4}$$

or more succinctly

$$\frac{d\rho'}{dt} = -\gamma\rho' \tag{B5}$$

Thus, from the expression for ρ' in terms of ordinates xz (Eq. 9)

$$\frac{d\rho'}{dt} = \rho' \ln(\lambda)\frac{dz}{dt} = -\gamma\rho' \tag{B6}$$

That is

$$\frac{dz}{dt} = -\frac{\gamma}{\ln(\lambda)} \tag{B7}$$

https://doi.org/10.5194/egusphere-2024-2520
Preprint. Discussion started: 4 November 2024

Author contributions. AWV devised the concept, developed the code and drafted the manuscript. AAV implemented the code, and participated in the manuscript development. AK implemented and validated the code, participated in the manuscript development, and curated the data and code to a public repository.

Competing interests. The contact author has declared that none of the authors has any competing interests

Acknowledgements. This work was supported by the Centre for Ocean Life, a Villum Kann Rasmussen Centre of Excellence supported by the Villum Foundation, by the Simons Foundation (grant 931976), and the European Union's Horizon 2020 research and innovation programme under grant agreements No 869383 (ECOTIP) and No 101083922 (Ocean-ICU).

https://doi.org/10.5194/egusphere-2024-2520
Preprint. Discussion started: 4 November 2024

References

Alldredge, A. L. and Gotschalk, C.: In situ settling behavior of marine snow, Limnology and Oceanography, 33, 339–351, https://doi.org/10.4319/lo.1988.33.3.0339, 1988.

Alldredge, A. L. and Gotschalk, C. C.: Direct observations of the mass flocculation of diatom blooms: characteristics, settling velocities and formation of diatom aggregates., Deep Sea Research Part Ii: Topical Studies in Oceanography, 36, 159–171, https://doi.org/10.1016/0198-0149(89)90131-3, 1989.

Alldredge, A. L., Granata, T. C., Gotschalk, C. C., and Dickey, T. D.: The physical strength of marine snow and its implications for particle disaggregation in the ocean, Limnology and Oceanography, 35, 1415–1428, 1990.

Andersen, K. H. and Visser, A. W.: From cell size and first principles to structure and function of unicellular plankton communities, Progress in Oceanography, 213, 102 995, 2023.

Azetsu-Scott, K. and Johnson, B. D.: Measuring physical characteristics of particles: A new method of simultaneous measurement for size, settling velocity and density of constituent matter, Deep Sea Research Part A. Oceanographic Research Papers, 39, 1057–1066, https://doi.org/10.1016/0198-0149(92)90039-v, 1992.

Azetsu-Scott, K. and Passow, U.: Ascending marine particles: Significance of transparent exopolymer particles (TEP) in the upper ocean, Limnology and oceanography, 49, 741–748, 2004.

Bach, L. T., Stange, P., Taucher, J., Achterberg, E. P., Algueró-Muñiz, M., Horn, H., Esposito, M., and Riebesell, U.: The influence of plankton community structure on sinking velocity and remineralization rate of marine aggregates, Global Biogeochemical Cycles, 33, 971–994, https://doi.org/10.1029/2019gb006256, 2019.

Banas, N. S.: Adding complex trophic interactions to a size-spectral plankton model: Emergent diversity patterns and limits on predictability, Ecological Modelling, 222, 2663–2675, https://doi.org/10.1016/j.ecolmodel.2011.05.018, 2011.

Belcher, A., Iversen, M., Giering, S., Riou, V., Henson, S. A., Berline, L., Guilloux, L., and Sanders, R.: Depth-resolved particle-associated microbial respiration in the northeast Atlantic, Biogeosciences, 13, 4927–4943, https://doi.org/10.5194/bg-13-4927-2016, 2016.

Boyd, P. W. and Newton, P.: Evidence of the potential influence of planktonic community structure on the interannual variability of particulate organic carbon flux, Deep Sea Research Part I: Oceanographic Research Papers, 42, 619–639, https://doi.org/10.1016/0967-0637(95)00017-Z, 1995.

Boyd, P. W., Claustre, H., Levy, M., Siegel, D. A., and Weber, T.: Multi-faceted particle pumps drive carbon sequestration in the ocean, Nature, 568, 327, https://doi.org/10.1038/s41586-019-1098-2, 2019.

Briggs, N., Dall'Olmo, G., and Claustre, H.: Major role of particle fragmentation in regulating biological sequestration of CO2 by the oceans, Science, 367, 791–793, 2020.

Buesseler, K. O., Lamborg, C. H., Boyd, P. W., Lam, P. J., Trull, T. W., Bidigare, R. R., Bishop, J. K. B., Casciotti, K. L., Dehairs, F., Elskens, M., Honda, M., Karl, D. M., Siegel, D. a., Silver, M. W., Steinberg, D. K., Valdes, J., Van Mooy, B., and Wilson, S.: Revisiting carbon flux through the ocean's twilight zone., Science, 316, 567–70, https://doi.org/10.1126/science.1137959, 2007.

Burd, A. B. and Jackson, G. A.: Particle aggregation, Annual Review of Marine Science, 1, 65–90, https://doi.org/10.1146/annurev.marine.010908.163904, 2009.

Cael, B. B., Cavan, E. L., and Britten, G. L.: Reconciling the size-dependence of marine particle sinking speed, Geophysical Research Letters, 48, e2020GL091 771, https://doi.org/10.1029/2020gl091771, 2021.

https://doi.org/10.5194/egusphere-2024-2520
Preprint. Discussion started: 4 November 2024

Carder, K. L., Steward, R. G., and Betzer, P. R.: In situ holographic measurements of the sizes and settling rates of oceanic particulates, Journal of Geophysical Research: Oceans, 87, 5681–5685, https://doi.org/10.1029/jc087ic08p05681, 1982.

Cavan, E. L. and Boyd, P. W.: Effect of anthropogenic warming on microbial respiration and particulate organic carbon export rates in the sub-Antarctic Southern Ocean, Aquatic Microbial Ecology, 82, 111–127, 2018.

Cavan, E. L., Trimmer, M., Shelley, F., and Sanders, R.: Remineralization of particulate organic carbon in an ocean oxygen minimum zone, Nature Communications, 8, 1–9, 2017.

Clift, R., Grace, J. R., and Webber, M. E.: Bubbles, Drops and Particles., Academic Press, San Diego, 1978.

DeVries, T., Liang, J., and Deutsch, C.: A mechanistic particle flux model applied to the oceanic phosphorus cycle, Biogeosciences, 11, 5381–5398, https://doi.org/10.5194/bg-11-5381-2014, 2014.

Diercks, A.-R. and Asper, V. L.: In situ settling speeds of marine snow aggregates below the mixed layer: Black Sea and Gulf of Mexico, Deep Sea Research Part I: Oceanographic Research Papers, 44, 385–398, https://doi.org/10.1016/s0967-0637(96)00104-5, 1997.

Dietrich, W. E.: Settling velocity of natural particles, Water Resources Research, 18, 1615–1626, 1982.

Dilling, L. and Alldredge, A. L.: Fragmentation of marine snow by swimming macrozooplankton: A new process impacting carbon cycling in the sea, Deep Sea Research Part I: Oceanographic Research Papers, 47, 1227–1245, 2000.

Ducklow, H. W., Steinberg, D. K., and Buesseler, K. O.: Upper Ocean Carbon Export and the Biological Pump, Oceanography, 14, 50–58, https://doi.org/10.5670/oceanog.2001.06, 2001.

Engel, A. and Schartau, M.: Influence of transparent exopolymer particles (TEP) on sinking velocity of Nitzschia closterium aggregates, Marine Ecology Progress Series, 182, 69–76, https://doi.org/10.3354/meps182069, 1999.

Engel, A., Abramson, L., Szlosek, J., Liu, Z., Stewart, G., Hirschberg, D., and Lee, C.: Investigating the effect of ballasting by CaCO3 in Emiliania huxleyi, II: Decomposition of particulate organic matter, Deep Sea Research Part Ii: Topical Studies in Oceanography, 56, 1408–1419, https://doi.org/10.1016/j.dsr2.2008.11.028, 2009.

Gibbs, R. J.: Estuarine flocs: their size, settling velocity and density, Journal of Geophysical Research: Oceans, 90, 3249–3251, https://doi.org/10.1029/jc090ic02p03249, 1985.

Gremion, G., Nadeau, L.-P., Dufresne, C., Schloss, I. R., Archambault, P., and Dumont, D.: A discrete interaction numerical model for coagulation and fragmentation of marine detritic particulate matter, Geosci. Model Dev. Discuss, 2021.

Guidi, L., Jackson, G. A., Stemmann, L., Miquel, J. C., Picheral, M., and Gorsky, G.: Relationship between particle size distribution and flux in the mesopelagic zone, Deep Sea Research Part I: Oceanographic Research Papers, 55, 1364–1374, https://doi.org/10.1016/j.dsr.2008.05.014, 2008.

Guidi, L., Stemmann, L., Jackson, G. A., Ibanez, F., Claustre, H., Legendre, L., Picheral, M., and Gorskya, G.: Effects of phytoplankton community on production, size, and export of large aggregates: A world-ocean analysis, Limnology and Oceanography, 54, 1951–1963, 2009.

Gärdes, A., Iversen, M. H., Grossart, H.-P., Passow, U., and Ullrich, M. S.: Diatom-associated bacteria are required for aggregation of Thalassiosira weissflogii, ISME Journal, 5, 436–445, https://doi.org/10.1038/ismej.2010.145, 2011.

Hayashi, Y., Wada, S., Seto, M., and Adachi, Y.: Cohesive bond strength of marine aggregates and its role in fragmentation, Frontiers in Marine Science, 10, 1167 169, 2023.

Hill, P. S., Syvitski, J. P., Cowan, E. A., and Powell, R. D.: In situ observations of floc settling velocities in Glacier Bay, Alaska, Marine Geology, 145, 85–94, https://doi.org/10.1016/s0025-3227(97)00109-6, 1998.

https://doi.org/10.5194/egusphere-2024-2520
Preprint. Discussion started: 4 November 2024

Iversen, M. H. and Lampitt, R. S.: Size does not matter after all: No evidence for a size-sinking relationship for marine snow, Progress in Oceanography, 189, 102 445, https://doi.org/10.1016/j.pocean.2020.102445, 2020.

Iversen, M. H. and Ploug, H.: Ballast minerals and the sinking carbon flux in the ocean: carbon-specific respiration rates and sinking velocity of marine snow aggregates, Biogeosciences, 7, 2613–2624, https://doi.org/10.5194/bg-7-2613-2010, 2010.

Iversen, M. H. and Ploug, H.: Temperature effects on carbon-specific respiration rate and sinking velocity of diatom aggregates–potential implications for deep ocean export processes, Biogeosciences, 10, 4073–4085, https://doi.org/10.5194/bg-10-4073-2013, 2013.

Iversen, M. H. and Robert, M. L.: Ballasting effects of smectite on aggregate formation and export from a natural plankton community, Marine Chemistry, 175, 18–27, https://doi.org/10.1016/j.marchem.2015.04.009, 2015.

Iversen, M. H., Nowald, N., Ploug, H., Jackson, G. A., and Fischer, G.: High resolution profiles of vertical particulate organic matter export off Cape Blanc, Mauritania: Degradation processes and ballasting effects, Deep Sea Research Part I: Oceanographic Research Papers, 57, 771–784, https://doi.org/10.1016/j.dsr.2010.03.007, 2010.

Jackson, G. A.: A model of the formation of marine algal flocs by physical coagulation processes, Deep Sea Research Part A. Oceanographic Research Papers, 37, 1197–1211, https://doi.org/10.1016/0198-0149(90)90038-w, 1990.

Jackson, G. A.: Using fractal scaling and two-dimensional particle size spectra to calculate coagulation rates for heterogeneous systems, Journal of Colloid and Interface Science, 202, 20–29, https://doi.org/10.1006/jcis.1998.5435, 1998.

Jackson, G. A.: Coagulation in a rotating cylinder, Limnology and Oceanography: Methods, 13, 194–201, 2015.

Jackson, G. A. and Burd, A. B.: Aggregation in the marine environment, Environmental Science & Technology, 32, 2805–2814, https://doi.org/10.1021/es980251w, 1998.

Jackson, G. A. and Burd, A. B.: Simulating aggregate dynamics in ocean biogeochemical models, Progress in Oceanography, 133, 55–65, https://doi.org/10.1016/j.pocean.2014.08.014, 2015.

Jokulsdottir, T. and Archer, D.: A stochastic, Lagrangian model of sinking biogenic aggregates in the ocean (SLAMS 1.0): model formulation, validation and sensitivity, Geoscientific Model Development, 9, 1455–1476, https://doi.org/10.5194/gmd-9-1455-2016, 2016.

Jouandet, M.-P., Trull, T. W., Guidi, L., Picheral, M., Ebersbach, F., Stemmann, L., and Blain, S.: Optical imaging of mesopelagic particles indicates deep carbon flux beneath a natural iron-fertilized bloom in the Southern Ocean, Limnology and Oceanography, 56, 1130–1140, https://doi.org/10.4319/lo.2011.56.3.1130, 2011.

Kajihara, M.: Settling velocity and porosity of large suspended particle, Journal of the Oceanographical Society of Japan, 27, 158–162, https://doi.org/10.1007/bf02109135, 1971.

Kiørboe, T.: Formation and fate of marine snow: small-scale processes with large-scale implications, Sci Mar, 65, 57–71, 2001.

Kriest, I. and Evans, G. T.: Representing phytoplankton aggregates in biogeochemical models, Deep Sea Research Part I: Oceanographic Research Papers, 46, 1841–1859, https://doi.org/10.1016/s0967-0637(99)00032-1, 1999.

Laurenceau-Cornec, E. C., Trull, T. W., Davies, D. M., De La Rocha, C. L., and Blain, S.: Phytoplankton morphology controls on marine snow sinking velocity, Marine Ecology Progress Series, 520, 35–56, https://doi.org/10.3354/meps11116, 2015.

Laurenceau-Cornec, E. C., Le Moigne, F. A., Gallinari, M., Moriceau, B., Toullec, J., Iversen, M. H., Engel, A., and De La Rocha, C. L.: New guidelines for the application of Stokes' models to the sinking velocity of marine aggregates, Limnology and Oceanography, 65, 1264–1285, https://doi.org/10.1002/lno.11388, 2020.

Lin, M., Lindsay, H., Weitz, D., Ball, R., Klein, R., and Meakin, P.: Universality in colloid aggregation, Nature, 339, 360–362, https://doi.org/10.1038/339360a0, 1989.

https://doi.org/10.5194/egusphere-2024-2520
Preprint. Discussion started: 4 November 2024

Logan, B. E. and Hunt, J. R.: Advantages to microbes of growth in permeable aggregates in marine systems 1, Limnology and Oceanography, 32, 1034–1048, https://doi.org/10.4319/lo.1987.32.5.1034, 1987.

Logan, B. E. and Wilkinson, D. B.: Fractal geometry of marine snow and other biological aggregates, Limnology and Oceanography, 35, 130–136, https://doi.org/10.4319/lo.1990.35.1.0130, 1990.

Loth, E.: Drag of non-spherical solid particles of regular and irregular shape, Powder Technology, 182, 342–353, https://doi.org/10.1016/j.powtec.2007.06.001, 2008.

Maerz, J., Six, K. D., Stemmler, I., Ahmerkamp, S., and Ilyina, T.: Microstructure and composition of marine aggregates as co-determinants for vertical particulate organic carbon transfer in the global ocean, Biogeosciences, 17, 1765–1803, https://doi.org/10.5194/bg-17-1765-2020, 2020.

McDonnell, A. M. and Buesseler, K. O.: Variability in the average sinking velocity of marine particles, Limnology and Oceanography, 55, 2085–2096, https://doi.org/10.4319/lo.2010.55.5.2085, 2010.

Meakin, P.: Fractal aggregates, Advances in Colloid and Interface Science, 28, 249–331, https://doi.org/10.1016/0001-8686(87)80016-7, 1987.

Miklasz, K. A. and Denny, M. W.: Diatom sinkings speeds: Improved predictions and insight from a modified Stokes' law, Limnology and Oceanography, 55, 2513–2525, 2010.

Mouw, C. B., Barnett, A., McKinley, G. A., Gloege, L., and Pilcher, D.: Phytoplankton size impact on export flux in the global ocean, Global Biogeochemical Cycles, 30, 1542–1562, https://doi.org/10.1002/2015gb005355, 2016.

Nowald, N., Fischer, G., Ratmeyer, V., Iversen, M., Reuter, C., and Wefer, G.: In-situ sinking speed measurements of marine snow aggregates acquired with a settling chamber mounted to the Cherokee ROV, pp. 1–6, IEEE, ISBN 1-4244-2522-0, https://doi.org/10.1109/oceanse.2009.5278186, 2009.

Parsons, T., Stephens, K., and Strickland, J.: On the chemical composition of eleven species of marine phytoplankters, Journal of the Fisheries Board of Canada, 18, 1001–1016, number: 6, 1961.

Reynolds, R. A. and Stramski, D.: Variability in Oceanic Particle Size Distributions and Estimation of Size Class Contributions Using a Non-parametric Approach, Journal of Geophysical Research: Oceans, 126, e2021JC017 946, 2021.

Serra-Pompei, C., Soudijn, F., Visser, A. W., Kiørboe, T., and Andersen, K. H.: A general size-and trait-based model of plankton communities, Progress in Oceanography, 189, 102 473, https://doi.org/10.1016/j.pocean.2020.102473, 2020.

Serra-Pompei, C., Ward, B. A., Pinti, J., Visser, A. W., Kiørboe, T., and Andersen, K. H.: Linking plankton size spectra and community composition to carbon export and its efficiency, Global Biogeochemical Cycles, p. e2021GB007275, 2022.

Sicko-Goad, L. M., Schelske, C. L., and Stoermer, E. F.: Estimation of intracellular carbon and silica content of diatoms from natural assemblages using morphometric techniques, Limnology and Oceanography, 29, 1170–1178, https://doi.org/10.4319/lo.1984.29.6.1170, 1984.

Smoluchowski, M. v.: Versuch einer mathematischen Theorie der Koagulationskinetik kolloider Lösungen, Zeitschrift für physikalische Chemie, 92, 129–168, 1918.

Song, Y. and Rau, M. J.: A novel method to study the fragmentation behavior of marine snow aggregates in controlled shear flow, Limnology and Oceanography: Methods, 20, 618–632, 2022.

Stemmann, L., Eloire, D., Sciandra, A., Jackson, G., Guidi, L., Picheral, M., and Gorsky, G.: Volume distribution for particles between 3.5 to 2000 µm in the upper 200 m region of the South Pacific Gyre, Biogeosciences, 5, 299–310, 2008.

https://doi.org/10.5194/egusphere-2024-2520
Preprint. Discussion started: 4 November 2024

Stokes, G. G.: On the effect of the internal friction of fluids on the motion of pendulums, Transactions of the Cambridge Philosophical Society, 9, 1851.

Syvitski, J. P., Asprey, K., and Leblanc, K.: In-situ characteristics of particles settling within a deep-water estuary, Deep Sea Research Part Ii: Topical Studies in Oceanography, 42, 223–256, https://doi.org/10.1016/0967-0645(95)00013-g, 1995.

Tappan, H. and Loeblich Jr, A. R.: Evolution of the oceanic plankton, Earth-Science Reviews, 9, 207–240, publisher: Elsevier, 1973.

Toktamış, D., Toktamış, H., and Yazıcı, A. N.: The effects of thermal treatments on the thermoluminescence properties of biogenic minerals present in the seashells, Radiation Effects and Defects in Solids, 171, 951–964, 2016.

Van der Jagt, H., Friese, C., Stuut, J. W., Fischer, G., and Iversen, M. H.: The ballasting effect of Saharan dust deposition on aggregate dynamics and carbon export: Aggregation, settling, and scavenging potential of marine snow, Limnology and Oceanography, 63, 1386–1394, https://doi.org/10.1002/lno.10779, 2018.

Visser, A., Saito, H., Saiz, E., and Kiørboe, T.: Observations of copepod feeding and vertical distribution under natural turbulent conditions in the North Sea, Marine Biology, 138, 1011–1019, 2001.

Visser, A. W. and Jónasdóttir, S. H.: Lipids, buoyancy and the seasonal vertical migration of Calanus finmarchicus, Fisheries Oceanography, 8, 100–106, 1999.

Volk, T. and Hoffert, M. I.: Ocean carbon pumps: Analysis of relative strengths and efficiencies in ocean-driven atmospheric CO2 changes, in: The carbon cycle and atmospheric CO2: natural variations Archean to present, vol. 32, pp. 99–110, American Geophysical Union, Washington DC, https://doi.org/10.1029/gm032p0099, 1985.

White, F. M.: Viscous Fluid Flow, McGraw-Hill, New York, NY, 1991.

Wiesner, M. R.: Kinetics of aggregate formation in rapid mix, Water Research, 26, 379–387, https://doi.org/10.1016/0043-1354(92)90035-3, 1992.

Zahnow, J. C., Maerz, J., and Feudel, U.: Particle-based modeling of aggregation and fragmentation processes: Fractal-like aggregates, Physica D: Nonlinear Phenomena, 240, 882–893, 2011.

https://doi.org/10.5194/egusphere-2024-2520
Preprint. Discussion started: 4 November 2024

Table 1. Estimated exponent $b \pm s$ for excess density vrs aggregate size power law where s is the 95% confidence interval. Δ_r is the $\log_{10} r$ range of aggregate size, and n the number of observations. References as given, and indicate field or lab studies.

b	$\pm s$	Δ_r	n		*reference*	
-0.38	1.21	0.5	14		Alldredge and Gotschalk (1989)	Field
-1.49	0.15	1.9	76		Alldredge and Gotschalk (1988)	Field
-2.09	1.22	0.5	13	i	Azetsu-Scott and Johnson (1992)	Field
-1.09	1.88	0.4	15	ii	–´´–	Lab
-0.72	0.20	0.8	37		Iversen et al. (2010)	Field
-0.83	0.55	0.9	104		Belcher et al. (2016)	Field
-1.11	0.94	0.8	10		Carder et al. (1982)	Field
-2.18	0.28	1.0	332		Diercks and Asper (1997)	Field
-1.07	0.09	1.2	294		Engel and Schartau (1999)	Lab
-1.21	0.05	1.1	20		Gibbs (1985)	Field
-1.46	0.05	1.6	1224		Chase 1979	Field
-1.13	0.14	1.1	63	i	Iversen and Ploug (2010)	Lab
-1.20	0.12	0.8	26	ii	–´´–	Lab
-1.01	0.20	0.5	97	iii	–´´–	Lab
-0.46	0.30	0.5	99		Hill et al. (1998)	Field
-0.51	0.23	0.9	187		Iversen and Ploug (2013)	Lab
-1.34	0.26	1.1	153		Iversen and Robert (2015)	Lab
-1.37	0.20	1.4	54		Kajihara (1971)	Field
-2.12	0.59	0.8	61	i	Laurenceau-Cornec et al. (2015)	Field
-1.24	0.21	0.8	59	ii	–´´–	Lab
-1.24	0.21	0.8	72	i	Laurenceau-Cornec et al. (2020)	Lab
-0.35	0.19	0.7	131	ii	–´´–	Lab
-1.53	0.12	1.2	274	i	Engel et al. (2009)	Lab
-1.07	0.09	1.2	249	ii	–´´–	Lab
-0.74	0.14	1.2	296	iii	–´´–	Field
-1.53	0.70	0.9	49		Nowald et al. (2009)	Field
-1.22	0.12	1.7	149		Syvitski et al. (1995)	Field
-0.95	0.37	1.3	57	i	Van der Jagt et al. (2018)	Field
-2.01	0.30	1.2	85	ii	–´´–	Field
-0.88	0.23	1.9	36		Guidi et al. (2008)	Field
-1.65	0.26	1.7	41		McDonnell and Buesseler (2010)	Field
-2.24	0.78	1.0	28		Jouandet et al. (2011)	Field
-1.59	0.02	1.2	1654		Bach et al. (2019)	Field
-0.11	0.25	0.7	36		Gärdes et al. (2011)	Lab
-1.74	0.27	1.4	154		Iversen and Lampitt (2020)	Field
-1.38	0.02	4.0	6332		All data points	-

https://doi.org/10.5194/egusphere-2024-2520
Preprint. Discussion started: 4 November 2024

Table 2. Glossary of variables, parameter settings for simulations and units.

variable	description	Value	Range	Units	
a	self similarity parameter	2	(1.8 – 2.1)	–	
α	stickiness	0.1	(0.02 – 0.3)	–	
ε	Turbulent dissipation rate	10^{-6}	(10^{-2} – 10^{-8})	$m^3 s^{-2}$	
$\overline{P}$	Total productivity	10^6	(10^5 – 10^7)	μgC m^2 day^{-1}	
$q_{m:c}$	Dry mass to carbon mass ratio	2.5		–	
h	Depth of simulated surface layer	20		m	
r	Aggregate raduis $r = r_o \delta^x$	–	r_o=1 to $r_{\max}$=10^6	μm	Eq. (9)
ρ	Aggregate density	–	(1000 to 1200)	kg m^{-3}	
ρ'	Aggregate excess density $\rho' = \rho - \rho_w = \rho_o \lambda^z \delta^{(a-3)x}$	–	ρ_o=1 to $\rho_{\max}$=200	kg m^{-3}	Eq. (9)
ρ_w	Density of seawater	1027		kg m^{-3}	
p	Agregate porosity	–		–	
ϕ	Aggregate solid mass volume fraction $\phi = 1 - p$	–		–	
m	Aggregate total mass $m = v\rho$	–		μg	
m'	Aggregate dry mass $m' = v\rho' + \phi v \rho_w$	–		μg	
w	Aggregate sinking speed	–		m day^{-1}	Eq. (4)
x	Radius bin ordinate	–	0 to X=30	–	
z	Density bin ordinate	–	0 to Z=15	–	
δ	Radius logarithmic interval $\delta = (r_{\max}/r_o)^{1/X}$	1.58		–	
λ	Excess density logarithmic interval $\lambda = (\rho_{\max}/\rho_o)^{1/Z}$	1.42		–	
ξ^{ij}	Aggregation transfer parameters $(i, j) \in [0, 1]$			–	Eq. (A3)
$N(x,z)$	Aggregate number density in state space	–		m^{-3}	
$M(x,z)$	Total dry mass of aggregates $M = Nm'$	–		μg m^{-3}	
$F(x,z)$	Aggregate sinking flux $F = Nm'w/q_{m:c}$	–		μgC m^{-2} day^{-1}	
$P(x,z)$	Size and density resolved productivity	–		μgC m^{-2} day^{-1}	
$\psi(x,z)$	State dependent fragmentation rate			day^{-1}	
β	Coaggulation Encounter kernal			m^3 day^{-1}	
γ	Remineralization rate	0.1		day^{-1}	
ψ_0	Fragmentation rate	0.5		day^{-1}	
g	Acceleration due to gravity	9.8		m s^{-2}	
C	Drag coefficient			day^{-1}	Eq. (5)
R	Reynolds number		< 100	–	
η	Kinematic viscosity of seawater	10^{-6}		$m^2 s^{-1}$	
v	Aggregate volume, $v = 4\pi r^3/3$			μm^3	